Heliyon 7 (2021) e08524

Contents lists available at ScienceDirect

Heliyon

journal homepage: www.cell.com/heliyon

Research article

A new cotton functionalized with iron(III) trimer-like metal framework as an effective strategy for the adsorption of triarylmethane dye: An insight into the dye adsorption processes

J.E. Conde-González [a], P. Lorenzo-Luis [b,c], V. Salvadó [d], J. Havel [e], E.M. Peña-Méndez [a,*]

[a] Departamento de Química, Unidad Departamental de Química Analítica, Facultad de Ciencias, Universidad de La Laguna, Tenerife, Spain
[b] Inorganic Chemistry Area, Section of Chemistry Faculty of Science, Tenerife, Spain
[c] Instituto Universitario de Bio-Orgánica "Antonio González", University of La Laguna, Tenerife, Spain
[d] Department de Química, Facultat de Ciències, Universitat de Girona, C/ Mª Aurèlia Capmany, 69, 17003 Girona, Spain
[e] Department of Chemistry, Faculty of Science, Masaryk University, Kamenice 5/A14, 625 00 Brno, Czech Republic

GRAPHICAL ABSTRACT

A new class of metal-framework containing commercial cotton is synthesized and characterized. Key features of this compound include complete stability in the presence of water as well as absorption data indicating that could be promising candidate to the removal of several triarylmetane dyes from aqueous solutions.

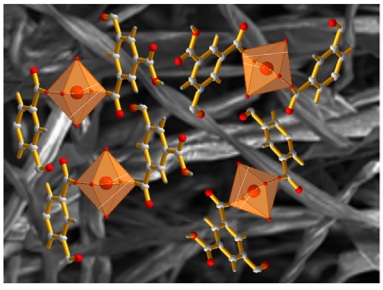

A new class of metal-framework containing commercial cotton is synthesized and characterized. Key features of this compound include complete stability in the presence of water as well as absorption data indicating that could be promising candidate to the removal of several triarylmetane dyes from aqueous solutions.

ARTICLE INFO

Keywords:
Natural cotton
Fe-BTC
Water
Solvation/desolvation penalty processes
Triphenylmetane dye
Adsorption

ABSTRACT

A new Cotton@Fe-BTC composite formed by Fe-BTC (BTC-H_3: trimesic acid) metal framework (Fe-BTC MOF loading as high 38 wt %) supported by cellulose fiber is synthesized in aqueous media using a simple and green preparation method, described for the first time in this manuscript. This new strategy relies on the synergetic effect of the pure cellulose and MOFs frameworks resulting in hybrid nanofibers of MOFs@cellulose composite. A complete characterization of the composite material reveals its structural similarity to MIL-100(Fe), a Fe-BTC material. The Cotton@Fe-BTC composite potential use as an eco-friendly and low-cost adsorbent was evaluated for its adsorptive performance for the removal of dye belonging to the triarylmethane dye family (Malachite Green (MQ), Brilliant Green (BG), Pararosaniline (PR), Basic Fuchsine (BF), Crystal Violet (CV), Methyl Green (Met-G), Victoria Blue B (VB), Acid Fuchsin (AF) and Aniline Blue (AB)) in aqueous solution. The fast kinetics and high dye removal efficiencies (>90%) obtained in aqueous solutions. The structure of Cotton@Fe-BTC network, contributed to the remarkable adsorption properties towards a variety of triphenylmethanedye. The interparticle studies showed two main steps in the dye adsorption processes, with the exception of AF and BG. The equilibrium adsorption capacities q_e (mg/g) follow the order: AF (3.64)<Met-G (3.70)<AB (4.87)<PR (5.52)<BF (5.76)< Met-G (7.22)<CV (9.63)<BG (16.34). However, going insight the adsorption mechanisms, it was remarkable the

* Corresponding author.
E-mail address: empena@ull.edu.es (E.M. Peña-Méndez).

https://doi.org/10.1016/j.heliyon.2021.e08524
Received 25 August 2021; Received in revised form 11 September 2021; Accepted 29 November 2021

finding that the reaction paths taking into account the influence of water molecules on the anionic dye adsorption, through the so-called solvation/desolvation penalty processes, may not be ignored. The easy preparation and manipulation of Cotton@Fe-BTC network as well as its stability and excellent performance for the adsorption makes this material a good candidate for a broad range of applications.

1. Introduction

The last decades, the detection of dye in samples from the industry, wastewater, and biological origin became to be one of the hot topics. Tons of dyeing wastewater from these industries is discharged into the environment every month [1, 2]. Worrying situation present two main faces: environmental pollution and life health damage. One class of the dye, which has received high attention due to their toxicity, are those belonging to the family of triarylmethane. Some of these dyes are known used for over a century, e.g., Crystal Violet or Brillant Green. They have found extensive applications in tropical medicine, textile, dying and paper printed, furniture industry, etc. Despite its extensive use, it is known that they can cause damage to liver, spleen, kidney and heart, inflicts lesions to skin, eyes, lungs and bones, and produces teratogenic effects to nervous system and brain [3]. Also, they colored the water affecting the living organisms, photosynthesis, promoting the bioaccumulation of non-desirable compounds, etc. The untreated effluents wastewaters are discharged to water bodies from urban wastewater, industrial effluents, etc. Therefore, it is essential to have a precise control about them on the environment. To have access to potable water is a human right, then to keep potable water reservoirs clean is of high demand. Different methodologies have been applied to remove dye pollutants from wastewater, however the results are economical non satisfactory [4]. Common methods for dye removal such as coagulation-flocculation, biological processes, oxidation processes are well reported in the literature. In addition, the determination of dye using different absorption techniques. Adsorption technology stands up among them. Due to its simplicity, easy used and high efficacy, this technology is considered to be one of the most effective and promising to clean dye from wastewater [5]. From activated carbon [6], zeolite [7], bentonite clay materials [8], has been studied as porous adsorbents to treat dyeing wastewater. However, these materials are not free of limitations, e.g., high cost and poor reusability are often hindering the large-scale use.

More efficient, low cost, and user-friendly systems for dye detection with low interference, high absorptivity and without the use of complex reagents, should be used. Furthermore, it is important to mention that the new adsorbents have found a niche of applications in the sample treatment process for the analytical determination of pollutants in water (e.g., solid phase extraction, dispersive solid phase extraction, etc.) [9, 10].

Among the plead of new synthesized sorbent materials, the network-framework approach (metal-organic framework MOFs structures) offers fascinating and interesting properties. Their structures are based on organic ligands as linkers and metal centers as the connectors, whereas their shape and pore size range from micro-to mesopore, permitting surface functionality. Some of these structures have shown broad diversity, in terms of activity, drug delivery, and mechanisms of action due to the combination of chemical and physical properties of the metal ions and the rich functionality of the organic ligands. Other weaker non-covalent attachments, such as hydrogen bonds, π-interactions and van der Waals forces, can also exert a strong influence on the structure and stability of the final coordination network [11, 12, 13]. However, the need for these frameworks to be stable, sustainable and recyclable materials is an obstacle to the introduction of easy and reproducible modifications. Considerable progress has been made in the theoretical prediction and network-based approaches to control the topology and geometries of the networks envisaging the production of functional materials. To the best of our knowledge, these compounds are essentially synthesized with 3d transition metal cations such as Fe, Co, Mn, Ni, Zn, Cu, Cd and 4f rare earths (Ho, Tm), coupled with flexible organic moieties (e.g., trimesic acid BTC-$H_n^{(3-n)-}$; n = 0,1,2) [14, 15, 16].

Cotton-based adsorbents were found to be considered viable for the treatment of organic and inorganic compounds polluted water via biosorption. However, the adsorption properties of the material are not good enough for complete resolving the undesirable water pollution. Then, to face the problem via enhancing the adsorption (uptake) of contaminants onto cotton adsorbents, various surface modifications approaches should be considered. In recent years, there has been an upsurge in the use of cellulose fiber, due to its unique chemical characteristics arising from the presence of hydroxyl groups including hemiacetal and acetal-links, allowing multiple intra- and inter-hydrogen bonds to form three-dimensional networks known as micro fibrillated cellulose (MFC) [17, 18]. Moreover, the activity of the surface of functionalized cellulose depends on the role of both the organic ligand and the metal ion and its behavior in a water medium, as shown in the first reported Cu-BTC network (called HKUST-1) on cellulosic substrates [19]. In fact, Abdelhameed and Emam *et al.*, have shown that it possible to functionalize cotton fabric by assembly with a Cu-BTC network with substantial sorbent activity, which is particularly effective in removing insecticides from wastewater [20]. Recently, Bao and *co-workers*, reported UiO-66 (Zr-MOFs) coated cotton fabricated for the extraction of trace-levels of phenoxy herbicides and phenolic acid compounds [21, 22]. In a later study Yang *et al.*, showed the feasibility of MOF@cotton fiber composite to adsorb U(VI) from aqueous solutions [23]. The use of pure cellulose in combination with MOFs frameworks in water or biphasic conditions provides a convenient strategy for separating the products from aqueous solution. This strategy has also been used in the preparation of recyclable photocatalyst composites of Ag_2WO_4@MIL-125-NH_2@cotton and Ag_3VO_4@MIL-125-NH_2@cotton applied to the degradation of dye in the visible light [24]. Some reviews have classified and discussed the most significant progress in the application of similar networks for the adsorption of organic dye from aqueous solution which are resistant to be degraded by light, heat, and oxidation in natural environments [25, 26, 27].

Nevertheless, to the best of our knowledge, until now, there has been no published data that summarizes the connection found between Fe^{3+}, BTC-H_3-linker and commercial cotton. To fill this gap, we present here an easy, cheap and eco-benign synthesis of the new Cotton@Fe-BTC network as a promising adsorbent to remove several triphenylmethane dye from aqueous solutions. The prepared Cotton@Fe-BTC was investigated by different characterization techniques. Kinetics and mechanism of adsorption of cationic and anionic dye were performed. The mechanisms of adsorption of the other dyes were suggested. To go insight the processes of dye adsorption, it may not be ignored that water is expected to interact with the metal organic framework through the center of the void. Thus, water relevance for the adsorption processes comes from its inherent properties as well as its structural, capacity of clusters formation and dynamic characteristics. Any discussion of water as a participant and responsible for the adsorption of e.g., anionic dye on the negative composite surface should begin with an acknowledgment that our understanding of water considered as a) media and b) participant in the adsorption process needs further studies. We considered the combination of these dual water faces mentioned above to understand the adsorption mechanisms of dye; together with different physic-chemical properties on the new material synthesized {dye-Cotton@Fe-BTC}, and the possible role of water molecules.

2. Material and methods

2.1. Reagents and solutions

All chemicals were of reagent grade and, unless otherwise stated, were commercially supplied. Natural cotton was purchased at a local

pharmacy. Iron (III) chloride hexahydrate and hydrochloric acid were purchased from Fluka Chemie AG, (Buchs, Switzerland). Iron (II) chlorate hexahydrate, ethanol (EtOH), methanol (MeOH), trimesic acid (benzene-1,3,5-tricarboxylic acid, H_3BTC), and sodium hydroxide were purchased from Sigma-Aldrich Chemie GmbH (Steinheim, Germany. Malachite green (MG; CAS 569-64-2); Brilliant Green (BG; CAS 633-03-4); Pararosaniline (PR, CAS 569-61-9); Basic fuchsine (BF; CAS 632-99-5); Crystal violet (CV; CAS 548-62-9); Methyl Green (Met-G; CAS 7114-03-6); Victoria Blue B (VB; CAS 2580-56-5); Acid Fuchsin (AF; CAS 3244-88-0) and Aniline blue (AB; CAS 66687-07-8) were purchased from Sigma-Aldrich. Deionized water was obtained using a Milli-Q gradient system A10 from Millipore (Bedford, MA, USA). Working solutions were prepared by appropriate dilution of the stock solution with ultrapure water. All chemicals were of analytical reagent grade unless otherwise indicated and were used as received without further purification and purchased from commercial sources. All glassware was rinsed with 10% nitric acid and Milli-Q water several times before use.

2.2. Preparation of Fe-BTC

Reported methods to obtain the Fe-BTC have been optimized but not methodology has been previously been reported for the loading of Fe-BTC on a cotton surface, leading us to propose the following new alternative protocol [14, 16, 28]. A mixture of ionized water/ethanol (1:1 v/v, 100 mL) containing $FeCl3^{\cdot 6H}2^{O}$ (1.86 g, 6.9 mmol) was added dropwise using a peristaltic pump, 1 mL min^{-1} to a solution of trimesic acid (1.65 g, 7.9 mmol) and triethylamine (0.3 mL) previously dissolved in 100 mL of water/ethanol (1:1 v/v) and stirred continuously for 1 h to ensure complete reaction. The resulting solution was centrifuged at 3500 rpm for 5 min and the light-brown solid obtained was washed twice with a cold water/ethanol mixture (1:1 v/v). The Fe-BTC MOF was collected and vacuum dried at room temperature. Finally, the material was grinded and sifted using an 0.125 mm sieve.

2.3. Preparation of Cotton@Fe-BTC composite

Cotton@Fe-BTC composite was prepared following an alternative synthetic strategy (Figure 1) to those previously reported for other Cotton@M-MOFs (M = Cu, Zr) [20, 21]. The cellulose fiber (natural cotton) was first washed with ethanol (40 mL), leaving this solvent to percolate before passing the iron solution (40 mL) through the cotton ensuring a minimum contact time of ~1 min. Once the iron solution had drained off, the cotton was washed with ionized water (40 mL). After allowing the washed cotton to dry, a BTC solution was added (40 mL) and the cotton was washed again with ionized water. The iron solution was then passed through the cotton again (40 mL) for 1 min, completing the first cycle. Eight cycles were performed to ensure the attachment of the Fe-BCT to the cotton. On finishing, the cotton was washed three times with ionized water (40 mL) and once with ethanol (40 mL). Finally, the Cotton@Fe-BTC composite was dried in an oven at 80 °C overnight (~20 h).

2.4. Adsorption test of dye on Cotton@Fe-BTC composite

Initially, amount of composite Cotton@Fe-BTC, dye concentrations were optimized. Due to the different dye adsorption onto Cotton@Fe-BTC, for comparison the following optimized conditions ($m_{mposite}$ = 0.050 g, C_{0dye} = 10 mg/L, V_{total} = 25 mL) for the kinetics study of the removal of selected triarylmethane dye from water. The amount of dye adsorbed by a gram of composite was calculated in accordance with Eq. (1),

$$q_t = \frac{V(C_0 - C_e)}{m} \quad (1)$$

where q_t is the amount of dye adsorbed at time t (min), V is the volume of the solution (mL), C_0 and C_e are the initial dye concentrations and at equilibrium dye concentrations (mg/·L), respectively, and m is the mass of composite fiber (g). The capacity of the adsorbent remained constant

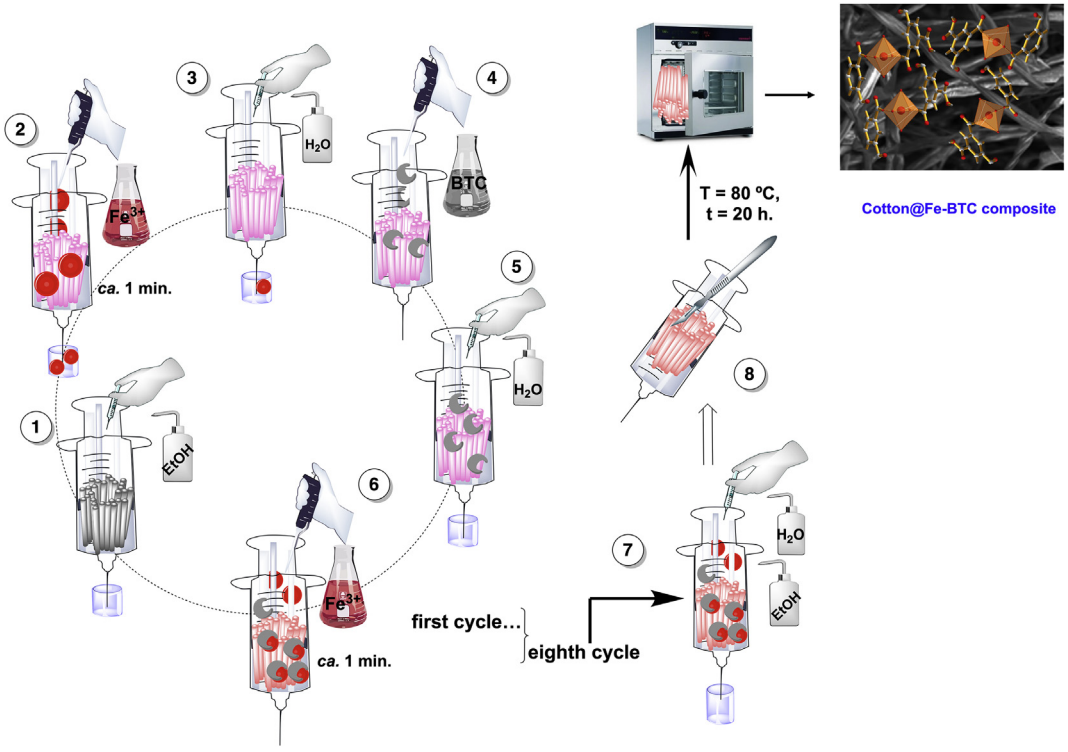

Figure 1. Schematic for illustrating the synthesis of Cotton@Fe-BTC composite under fully sustainable conditions.

for the first five times but then dropped to less than 70%. The experiments were run in triplicate and values that deviated from the relative standard deviation (RSD) > 5% were repeated. The adsorption kinetic experiments were also run-in batch mode with the same experimental conditions and pseudo-first order, pseudo-second-order and the interparticle diffusion models were applied for an in-depth insight into the adsorption mechanisms using Eqs. (2), (3), and (4), respectively,

$$\log(Q_e - Q_t) = \log Q_e - \frac{k_1}{2.303} t \quad (2)$$

$$\frac{t}{Q_t} = \frac{1}{k_2 Q_e^2} + \frac{1}{Q_e} t \quad (3)$$

$$Q_t = C + k_i t^{0.5} \quad (4)$$

where Qe (mg·g^{-1}) and Q_t (mg·g^{-1}) are the quantity of dye removed per mass (g) of dye at equilibrium, and at the time, t (min), respectively, and K_1 (min^{-1}) is the pseudo-first-order rate constants Q_t and Q_e (mg/g) and t (min) are as defined above and k_2 (mg/g) is the pseudo-second-order rate constant; k_i is the intraparticle diffusion rate constant and C represents the related kinetic parameter. The adsorption tests of dye onto Cotton@Fe-BTC composite were performed in aqueous solution (range of pH = 6.02–6.44, 298 K). First of all, continuous flow adsorption experiments were carried out on a pipette-tip packed with Cotton@Fe-BTC composite acting as the extracting column and the process was monitored in real time using UV/vis spectroscopy. The equilibrium adsorption data obtained were evaluated using different monolayer and multilayer models (Langmuir, Freundlich, Brunauer-Emmett-Teller (BET), McMillan-Teller (MET), Khan and Koble-Corrigen). The reusability of the material was studied evaluating the capacity of the adsorbent.

2.5. Kinetic study

The parameter saturation (%) was calculated according to:

$$Saturation\ (\%) = \frac{D + \delta(f-1)}{D} \cdot 100 \quad (5)$$

$$f = 1 - \frac{t_f}{t_\delta} = \frac{M_\delta}{(v_x - v_b) \cdot C_0} \quad (6)$$

were calculated from the obtained breakthrough curves using the following mathematical expressions. Where f is the fractional capacity of the column (equation 6), δ primary adsorption zone, and D effective diffusion coefficient.

2.6. Structural characterization

X-ray powder diffraction patterns were obtained using a PANalytical Empyrean diffractometer with non-monochromatic Cu-radiation [λ(CuKα1) = 1.5406 A, λ(CuKα2) = 1.5444 A]. A PIXcel Medipix3 detector in a scanning line mode was used with an active length of 3.3473° in 2θ over the 5 ≤ 2θ ≤ 80° range, with a step size of 0.026° and a time per step of 60 s. FTIR spectra were recorded on an Agilent Cary 630 IR spectrometer equipped with diamond attenuated total reflectance (ATR). Thermograms of TGA and DSC were obtained using a simultaneous TGA/DSC Discovery SDT 650 (TA Instruments). Measurements were performed with hermetically crimped Tzero aluminum crucibles (40 μL, ~5 mg of samples) under nitrogen atmosphere at a flow rate of 50 mL/min^{-1} from 26 to 550 °C (at a heating rate of 10 °C min^{-1}). The number of decomposition steps was identified using the derivative thermogravimetric curve (DTG). Elemental analysis (C, H) was performed with a LECO CHNS TruSpecMicro automatic analyzer. The particle size distribution and zeta-potential were measured at different pH values using a Malvern Zetasizer Nano ZS, Micromeritics AUTOCHEM 2920, a pH meter equipped with an Inlab® micro-pH electrode (Mettler Toledo, Barcelona, Spain), and an IKA Labourtechnik RCT B S1 stirrer-hot plate (IKA, Staufen, Germany). The specific surface area, pore size distribution, and pore volume were measured by the Brunauer, Emmett and Teller method (BET) and a surface area analyzer at 77 K in the range of 0.02 ≤ P/P0 ≤ 1.00 on a Gemini V 2365 Model (Micrometrics, Norcross, GA, USA). The morphologies of the synthesized Cotton@Fe-BTC composite were characterized using a scanning electron microscope (SEMQUANTA FEI 200 FEG-ESEM) and energy-dispersive X-ray spectroscopy (EDX), operating at an accelerated voltage of 10 kV (spot 3.5, WD 10mm, 60Pa) at the required magnification at room temperature. The same microscope equipped with an energy dispersive X-ray spectrometer (EDX) was used with a field emission gun for mapping and determining the surface elemental composition.

3. Results and discussion

The success of the strategy used to functionalize the natural cotton surface by Fe-BTC explained in the Experimental Section (Figure 1) was confirmed by XRD and FTIR analyses. Figure 2 displays the framework topology for cotton and Cotton@Fe-BTC. An incipient shoulder and a maximum peak, which are characteristic of diffraction peaks of (101) and (101) lattice planes for cellulose type I, are present at 2θ = 14.8 and 16.5°, respectively. Similarly, the diffraction peak of natural cotton (2θ = 22.6°), assigned to (002) lattice plane of cellulose type I, was also observed for Cotton@Fe-BTC. The broad peak ca. 2θ = 34° observed for Cotton@Fe-BTC seems to indicate a possible bond to the trivalent metal [19, 20, 29]. It is important to stress, that the combination of the two components of this MOF, the metal ion and the organic linker, provides a low resolution of the presented XRD pattern due a semi-amorphous nature of this material [30, 31]. Figure 3, show the conformational environment of BTC linker molecules as vibrations in the 700-1720 cm^{-1} range which is the characteristic region for its identification [16, 32]. On the other hand, a broad band centered at 3404 cm^{-1} due to the stretching frequency of the OH group; a band at 2899 cm^{-1} related to the asymmetric C–H stretching vibration that can be assigned to the cellulose in cotton; bands placed at 1191 and 1143 cm^{-1} which are assigned to the asymmetric bridge C–O–C; and the broad signal observed at 1023 cm^{-1} corresponding to O–C stretching. Evaluation the FTIR spectra before and after the functionalization of the natural cotton shows the presence of a band at 1582 cm^{-1}, corresponding to asymmetric stretching vibrations of O–C=O BTC linker. This fact confirmed that the interaction between cotton and Fe-BTC takes place through the –COOH and –OH groups of natural cotton and iron ions [16, 20]. Comparing cotton and Cotton@-FeBTC those signals corresponding to O–H and C=O groups (1720 cm^{-1}) become weakened and difference between the strength of the C=O and C–O bonds decreases. Also, given the conjugation of the carbonyl group with the benzene ring, the C=O modes are detected at wavenumbers higher than non-conjugated C–O modes, confirming successful coordination [16, 32].

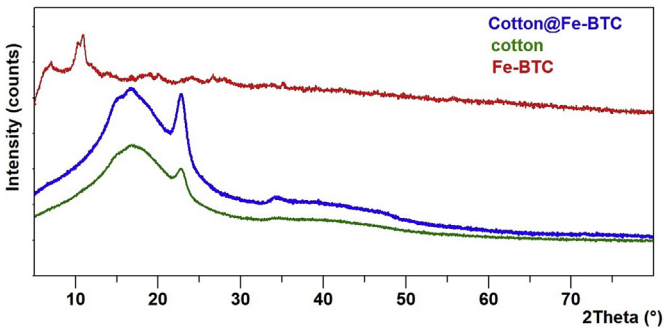

Figure 2. X-ray powder diffraction patterns: Basolite®F300 (Fe-BTC); natural cotton and Cotton@Fe-BTC composite.

It should be noted that glucose is a monomer that forms a cellulose via a condensation polymerization process, where each hydroxyl group has a more acidic character (more δ^+) than a typical alcohol group, due to the oxygen atoms (including hemiacetal and acetal-link ones), allowing multiple intra- and inter-hydrogen bonds in the cellulose fiber [17] (Figure 4a). In line with this, the IR spectrum of the Cotton@Fe-BTC (Figure 3) shows Fe–OH and Fe–OH_2 stretching (670-1100 cm^{-1}) as a result of the hydration of the material [16, 33].

In order to unambiguously establish the -COO^--carboxylate coordination mode to iron ions, we have compared the structural features of synthesized Fe-BTC with mesoporous MIL-100(Fe), a known Fe-BTC MOF [Fe_3O F-$(H_2O)_2((CO_2)_3C_6H_3)_2nH_2O$, n ≈ 14], which is formed with the same linker and Fe(III) ion within the octahedron [35, 36]. A survey to the literature shows that the assembling of the Fe-BTC MOF [$Fe_3O(OH)(H_2O)_2$-$[C_6H_3(CO_2)_3]_2$], is based on hybrid supertetrahedra built up from iron octahedral [Fe_3-μ_3O], which contain coordinatively unsaturated metal sites (CUSs) of amphiphilic character [34] (Figure 4b). The assembling of these hybrid supertetrahedra, allows to water to be adsorbed on acid sites where it is coordinatively attached *via* its oxygen atom. Additional information regarding the composition of Fe-BTC, elemental analyses and a thermal study have been performed together with those of cotton and Cotton@Fe-BTC for comparison purposes. It is important to stress, that the synthesis of the composite yields a Fe-BTC loading as high as 38 wt % for Cotton@Fe-BTC. Thermal analysis (Figure 5 and Table 1), shows two overlapped weight losses between 28 and 495 °C [DTG_{peak} at 89 and 469 °C, respectively]. The first (~30.5%) between 28 and 197 °C, is attributed to the evaporation of solvated and coordination water molecules and to network decomposition. The second weight loss (~28.4%) between 197 and at 495 °C, is attributed to the phenyl groups, which results in the collapse of the lattice structure [37]. This suggests that the use of water as a media is beneficial for its network stability [38, 39] (hydrated protons $[H(H_2O)_n]^+$, Figure 4b).

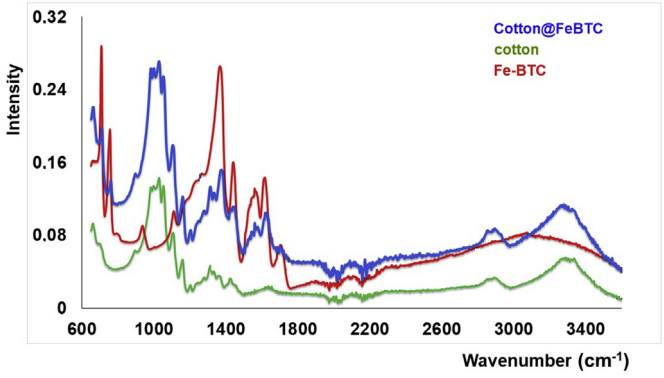

Figure 3. FTIR spectra of Basolite®F300 (Fe-BTC); natural cotton and Cotton@Fe-BTC composite.

The final products were not characterized, although it is evident that Fe_xO_y was formed. On the other hand, elemental analysis indicated that the contents of C and H (obs: 21.46% C, 3.81% H) are in agreement with the values based on the structure formula, $[Fe_3O(OH)(H_2O)_2$-$\{C_6H_3(CO_2)_3\}_2]\cdot nH_2O$ (M_w = 920.4 g mol^{-1}: 23.45 % C, 4.45 % H; 18.19 % Fe; n = 15), according from the reported structure formula $[Fe_3O(OH)(H_2O)$-$\{C_6H_3(CO_2)_3\}_2]\cdot nH_2O$ (24 % C, 19 % Fe, n ≈ 14) [16]. It is important to point out the excess of carbon content, as well as that the water content deduced from the structure determination (29.33 %) is slightly lower than the experimental value (TG-DTG, 30.50 %, n = 15.6).

The characterization of the new material was performed by SEM and EDX techniques to observe the surface morphology, pore textural properties and composition. The images obtained by SEM for pristine natural cotton were used as a reference (Figures 6a, b). The SEM images depicted in Figures 6c, d show the uniformity of the Fe-BTC on the cellulose cotton fiber surface.

The presence of iron-ions on the cellulose fiber surface is particularly interesting. The mapping SEM images (Figures 7a,b) show that C, O and Fe are uniformly distributed on the cellulose fiber surface, as is confirmed by the element mapping images (Figure 7c). Quantitative analysis of the resulting maps showed an average iron atomic content of 15.95 % on the surface of the cellulose fiber, indicating interaction of the cellulose fiber surface with the Fe-BTC. Comparably, the morphology of the Cotton@Fe-BTC composite is significantly more crystalline than Basolite®F300. This result is confirmed by quantitative results obtained by N_2 adsorption/desorption isotherms, as presented thereafter.These observations further confirm the significant role of cellulose fiber as a macro-molecule building unit in the Cotton@Fe-BTC composite preparation.

The properties described above were completed with the pore diameter distribution and surface area determined from N_2 adsorption/desorption isotherms using natural cotton as a reference. It can be seen from Figure 8 that a mass of Fe-BTC is successfully anchored on the surface of cellulosic fiber. On the other hand, the surface areas estimated using the BET method were 8.33 and 1.44 m^2/g, respectively, in good agreement with the Langmuir surface area values obtained (11.62 and 1.90 m^2/g, respectively). The slightly higher surface area can be explained by its nano character, rather than by it being a poor-quality material. The other remarkable feature of this isotherm is the amount of N_2 adsorbed at P/P_o beyond 0.1 (in the mesopore range), which

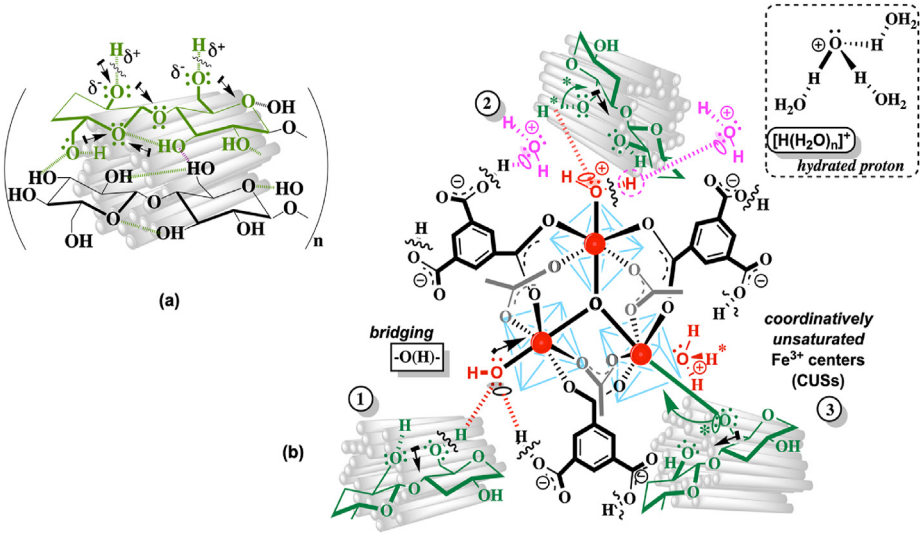

Figure 4. (a) Parallel cellulose fiber chain segment showing polarization effect around OH- groups ($\delta^{+,-}$) via natural inductive effect ($_+$I) allowing multiple intra- and inter-hydrogen bonds in the cellulose fiber (green dashed lines). (b) Hybrid supertetrahedra built Fe-BTC MOF $[Fe_3O(OH)(H_2O)_2$-$[C_6H_3(CO_2)_3]_2]$: proposed pathways (path 1) ([Fe-μ_3O]-O(H)····H, red dashed line); (path 2) ([Fe-μ_3O]-(H_2O)····H, red/magenta dashed lines allowing hydrated protons $[H(H_2O)_n]^+$. Finally, (path 3) a highly stable coordination bond ([Fe-μ_3O]-O) (are called CUSs-moiety, green line) (Adapted from Refs. [17, 34]).

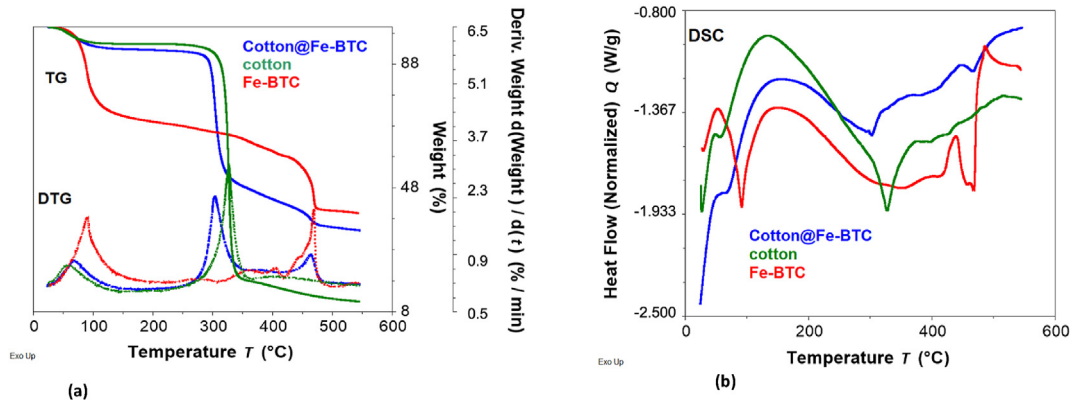

Figure 5. TG-DTG curves (a) and DSC curves (b): Basolite®F300 (Fe-BTC); natural cotton and Cotton@Fe-BTC composite.

Table 1. Thermal data of the samples under N_2 atmosphere.

First step			
Sample	ΔT (°C)	DTG_{peak}(°C)	DSC $_{Tonset}$(°C)
Cotton@Fe-BTC	25–150	67	67
Fe-BTC	28–197	89	91
Cotton	27–149	59	26; 56
Second step			
Sample	**ΔT (°C)**	**DTG_{peak}(°C)**	**DSC_{peak}(°C)**
Cotton@Fe-BTC	150–493	303,464	302, 465
Fe-BTC	197–495	495	438,487
Cotton	149–391	327	327

became as high as that adsorbed in the intermediate mesopores and micropores range and in accordance with the presence of voids between the particles ($P/P_0 > 0.8$) [40, 41, 42].

3.1. An insight into Cotton@Fe-BTC adsorption properties

Nine triarylmethane dye were selected as a model of contaminants to examine the performance of Cotton@Fe-BTC as a sorbent for the removal of small molecules (Figure 9). As depicted in Figure 10, the continuous flow adsorption experiments were conducted on a pipette-tip, packed with Cotton@Fe-BTC, acting as the extracting column and the process was monitored in real-time using UV/vis spectroscopy.

Factors such as contact time, temperature, amount of adsorbent, concentration of the adsorbate, and initial pH can affect the adsorption process [43]. In this work, the experiments were run at room temperature and the pH was that which corresponded to the dye aqueous solution (Table 2) whereas the dye concentration (10 mg/L) and the amount of adsorbent (50 mg) were not varied. Our previously published results have shown that the surface charge of Fe-BTC MOF is negative under experimental conditions with similar pH values ($pH_{pzc} = ca.$ 3.2) [28]. In these conditions there was significant uptake of most of the dye molecules. Hence, using the pipette-tip packed with Cotton@Fe-BTC,

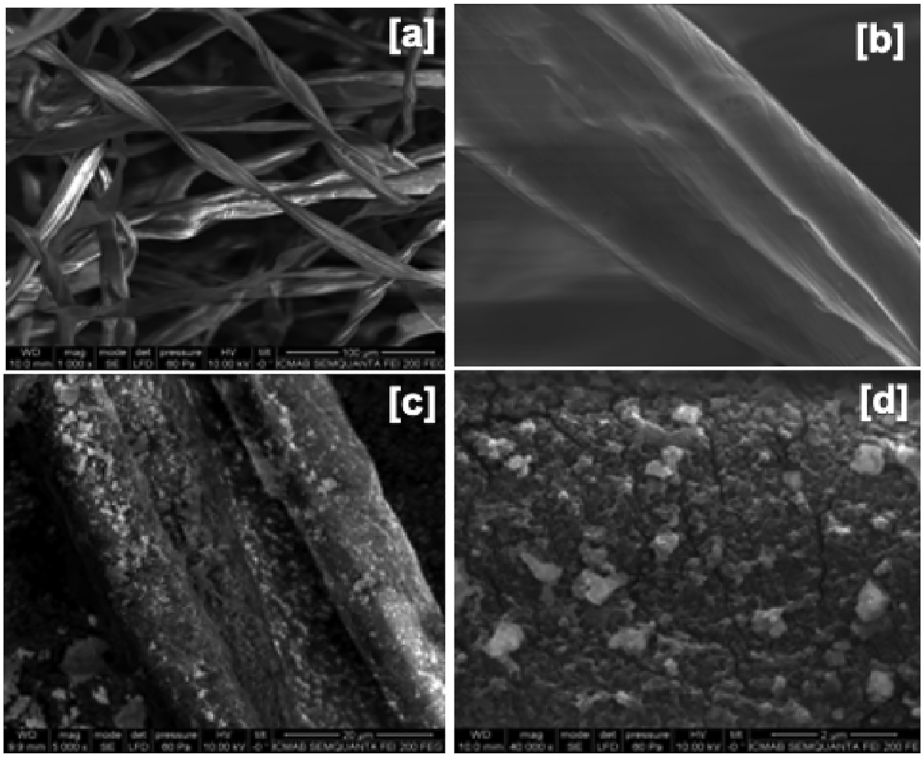

Figure 6. SEM images: (a, b) for reference pristine cotton fibers; (c,d) Fe-BTC linked onto cellulose fiber surface.

breakthrough at 90% (mg/g) retained dye was achieved: 10.70 (BG), 9.20 (CV), 5.51 (Met-G), 4.29 (BF), 4.01 (MG), 2.36 (PR), 3.47 (AB), 2.81 (VB), and 0.02 (AF).

Under these comparable running experimental conditions ($pH_{average\ value} = 6.25$), the water molecules play a leading role due to the effect of solvation/desolvation penalty processes on the adsorption/desorption of specific dye molecules [44]. It cannot be ignored that water acts as a nucleophile (spacefill) and as a donor of hydrogen of up to two bridges, as well as an acceptor of the hydrogen atom in the interaction with other water molecules (Figure 11) Then, it mediates electrostatic interactions [26, 27].

As depicted in Figure 11, the dissociation process of diamino- and triamino-derivatives can occur by removing the counter ions, affording the cationic and anionic species. Other possible interactions that may take place in aqueous medium are proposed. Whereas phenyl groups have low migratory aptitudes, they also have higher charge densities, decreasing the ability of the $–NH_2$-moiety to form hydrogen bonds. Furthermore, the amino groups ($Ph–NH_2$) are the basic part of a conjugate acid-base pair, in which the acid is the protonated ammonium cation ($Ph\text{-}NH_3^+$; $pKa_{(NH3)} \sim 9$), allowing interactions between charge-charge and the solvation process. Therefore, at working pH values, the remaining $–NH_2$ form is not protonated. Likewise, the reaction between water molecules and sulfonic acid groups (pKa = -2.8) increases the hydrophilic character of the molecules, the hydrogen-

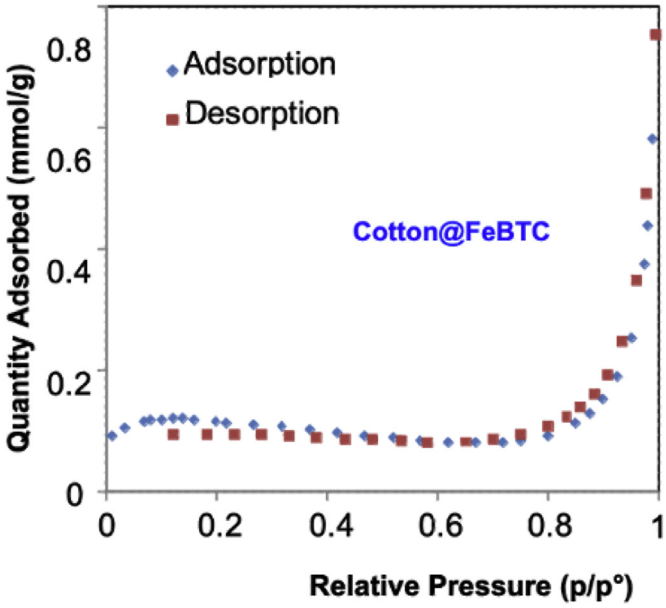

Figure 8. N_2 adsorption/desorption isotherms of Cotton@Fe-BTC composite.

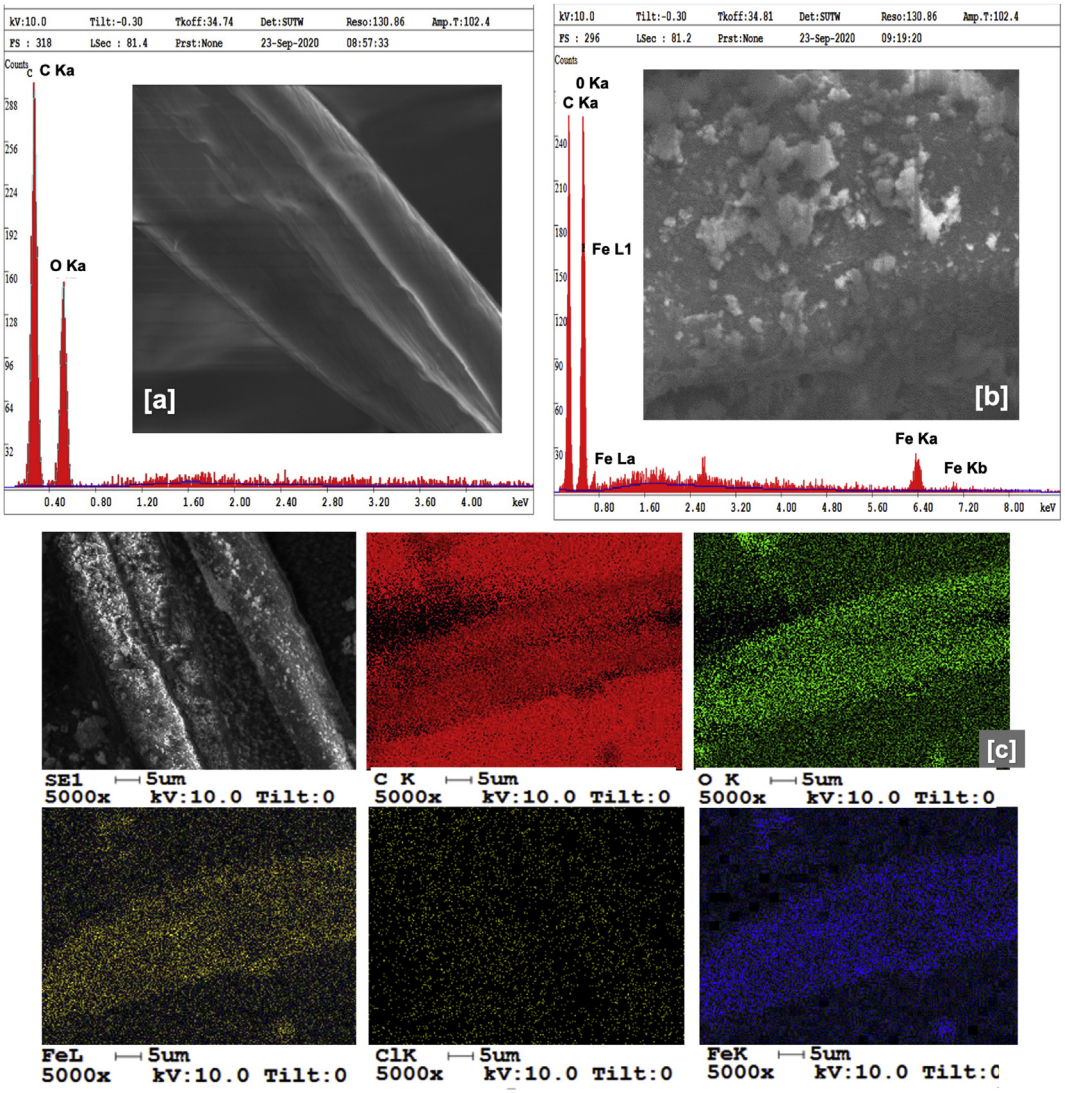

Figure 7. SEM image: (a,b) reference pristine cotton fiber and fiber Cotton@Fe-BTC composite; (c) EDS element mapping images.

bonding interactions and ion channels. Nevertheless, the acidic proton could easily be released to form hydrated proton species $[H(H_2O)_n]^+$ in the aqueous media (Figure 4b). The results described above suggest that the adsorption mechanisms of dye onto the Cotton@Fe-BTC composite imply intense electrostatic interactions such as those between oppositely charged species. As these species are solvated in the aqueous media, desolvation is needed to favor the interaction between the Cotton@Fe-BTC surface and the dye [44, 45, 46]. The ease of desolvation may affect the nature of binding and, hence, solvation/desolvation penalty has an essential effect on the dye adsorption process. The low adsorption capacity of Cotton@Fe-BTC for acid fuchsin (AF) in comparison with the other studied dye may mainly be caused by dipole-induced dipole interactions between Ph-SO_3^- moiety and the $[H(H_2O)_n]^+$ species formed with the water molecules of the solvent, which also lead to repulsion interactions with the Cotton@Fe-BTC surface. These repulsion interactions are much stronger than those corresponding to the charge-charge interactions between Ph-NH_3^+ and $^-$OOC-. On the other hand, the inductive effect ($_+$I) of the alkyl groups bound to nitrogen and the solvation effect of the iminium cation in particular, restrain the interaction between the composite and the dye. It is noteworthy that short alkyl group chains bound to nitrogen will favors the solvation effect more than long alkyl group chains. The cationic portion of the dye contains iminium ion with a pendant methyl or ethyl group, which makes the surface hydrophobic [44, 45, 46].

Thus, the mechanisms involved in the adsorption dye onto Cotton@Fe-BTC composite may be mainly due to the more intense electrostatic interactions between the oppositely charged species or dipoles. In the case of the charged species, a significant desolvation penalty should be considered.

3.2. Kinetic study

The kinetic study sheds light on the adsorption mechanisms and the uptake rate of anionic and cationic dye by Cotton@Fe-BTC composite (Table 2, Figures 9 and 12). The kinetic study of the adsorption experiments was carried out in batch mode under the conditions described in the Experimental Section [47]. The adsorption processes onto the composite were very fast for all dye, reaching equilibrium values in <20 min. The BG adsorption increased dramatically in less

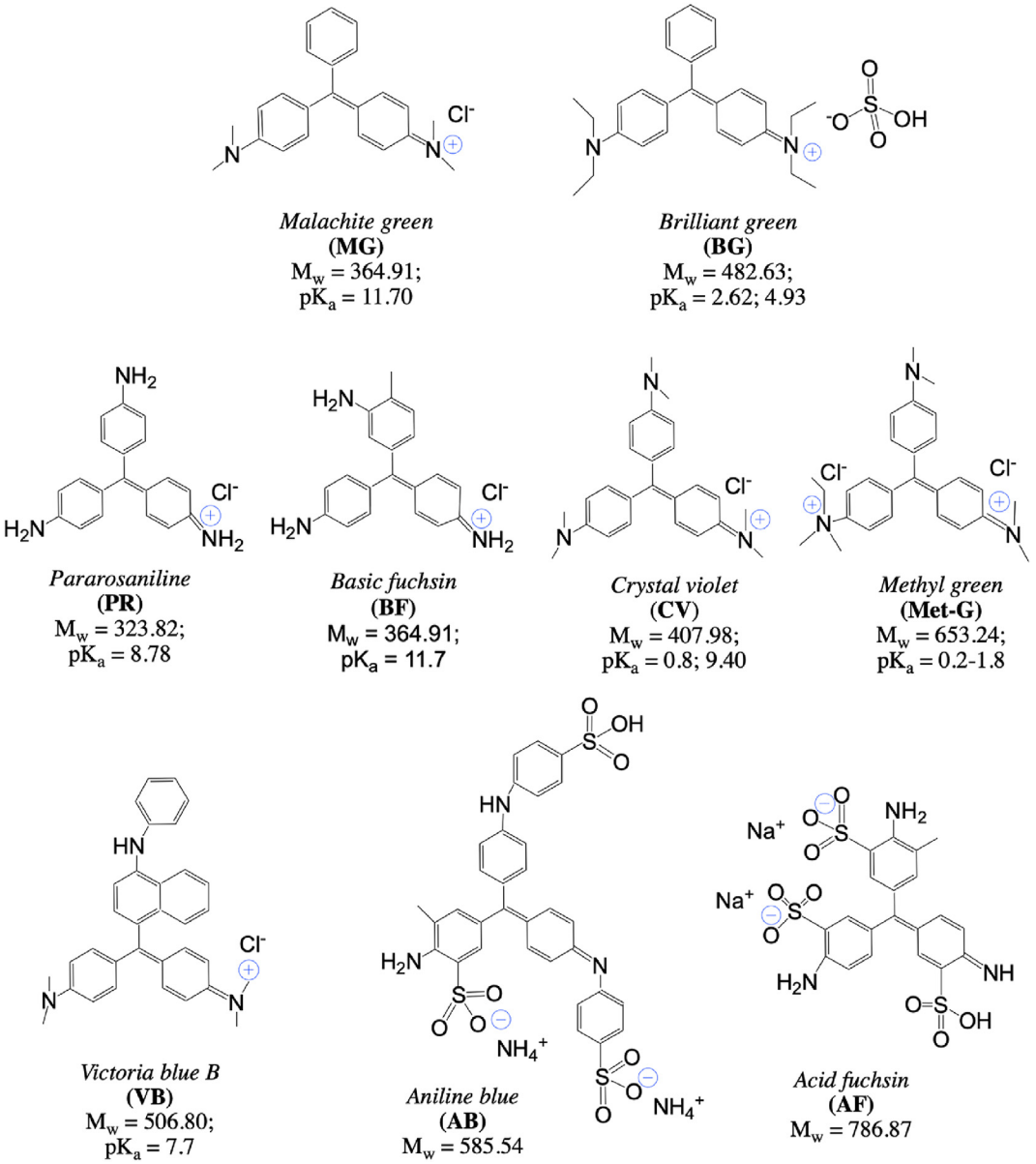

Figure 9. Structures of diamino and triamino derivatives of triarylmethane selected (are called malachite green series and magenta series, respectively).

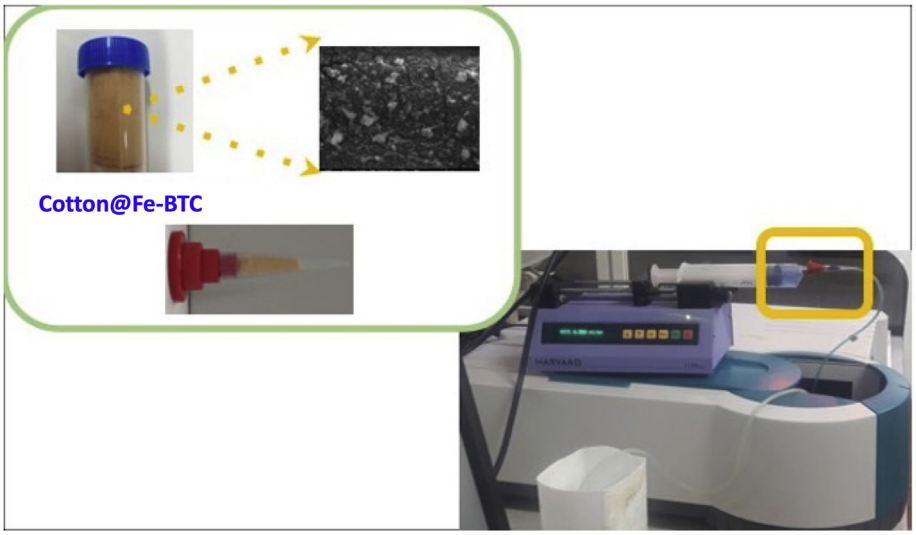

Figure 10. Experimental procedure for probing the Cotton@Fe-BTC composite performance for dye small molecules adsorption. Inset, SEM-picture of Fe-BTC linked onto cellulose fibers surface (top left) and a detail of on-tip system (lower right corner).

than 1 min of coming into contact with the modified cotton material, having the fastest adsorption among the studied dye (Figure 13).

The kinetic data of the dye molecules in aqueous solution, whose initial pHs ranged from 6.02 to 6.44 (Table 2), at 298 K were analyzed using the pseudo-first-order, pseudo-second-order and intra-particle diffusion kinetic models. The selection of the model that best fitted the experimental data was based on the linear regression determination coefficient (R2), and kinetic parameters were then calculated from the selected model. The Weber–Morris model (intra-particle diffusion model) was employed to more thoroughly understand the adsorption mechanisms of the chosen family of triarylmethane dye by the synthesized Cotton@Fe-BTC fibers. The results obtained show that more than one mechanism controlled the uptake by Cotton@Fe-BTC, rather than the possible diffusion of the studied dye.

Table 2. Parameters of the experimental kinetic models.

Dye	$pH_{initial}$	Model	R^2	k_1 (L/min)	q_e(mg/g)
First step					
MG	6.44	Pseudo-first	0.9967	0.149	3.60
BG	6.33	Fast-adsorption	—	—	—
PR	6.08	Pseudo-first	0.9954	0.183	5.29
BF	6.02	Pseudo-first	0.9935	0.131	5.74
CV	6.44	Pseudo-second	0.9991	0.010	7.06
Met-G	6.20	Pseudo-first	0.9994	0.193	7.03
VB	6.22	Pseudo-second	0.9998	0.006	14.7
AB	6.15	Pseudo-first	0.9988	0.311	5.29
AF	6.36	Pseudo-second	0.9970	0.158	4.64
Second step					
MG	6.44	Pseudo-second	0.9992	0.095	3.70
BG	6.33	—	—	—	—
PR	6.08	Pseudo-second	0.9996	0.070	5.52
BF	6.02	Pseudo-second	0.9962	0.038	5.76
CV	6.44	Pseudo-second	0.9980	0.030	9.63
Met-G	6.20	Pseudo-second	0.9982	0.045	7.22
VB	6.22	Pseudo-second	0.9992	0.047	16.3
AB	6.15	Pseudo-second	0.9978	0.282	4.87
AF	6.36	—	—	—	—

R^2 determination coefficient.

As can be seen in Figure 12, the kinetic data for each dye is represented by two segments, suggesting that the dye adsorption process onto Cotton@Fe-BTC proceeded in two steps involving surface sorption and intraparticle diffusion [48]. In the first main segment, for the cationic dye (MG, PR, BF and Met-G) and AB anionic dye, the kinetic data fitted with the pseudo first-order model ($R^2 > 0.9930$) whilst cationic dye CV, VB and anionic dye AF showed a better fit of the experimental data with the pseudo second-order model ($R^2 > 0.9970$), being chemisorption the rate-limiting step. As is described above the interaction may be driven by solvation effects (Figure 11). The adsorption capacities (q_e, mg/g), follow the order: AF (4.64) < CV (7.06) < VB (14.7). In the case of Brilliant Green (BG), the dye was adsorbed in less than 1 min of coming into contact with the network surface (Table 2) and its behavior may be related to a pseudo-first-order heterogeneous reaction [49]. The rapid uptake at the earlier contact time could be ascribed to the fact that its long alkyl group bound to nitrogen does not assist the solvation effect. Due to the fast velocity of the adsorption process, the reaction rate constant could not be measured. As for the second main segment, the kinetic study suggests that the adsorption onto Cotton@Fe-BTC follows the pseudo-second-order model for most of the dye (Table 2), indicating the importance of chemisorption [50, 51]. The equilibrium adsorption capacities q_e (mg/g) follow the order: MG (3.70) < AB (4.87) < PR (5.52) < BF (5.76) < Met-G (7.22) < CV (9.63) < BG (16.34). The kinetic obtained for AF anionic dye with the intraparticle diffusion model (q_e 3.64 mg/g) is an exception that suggests a different adsorption mechanism.

3.3. Adsorption isotherms

Adsorption isotherms experiments were performed to characterize the adsorption of selected dye of the triarylmethane family at the pH of the dye aqueous solutions (Table 2) and to obtain information about the nature of the interaction of the dye on the Cotton@Fe-BTC [52, 53]. Different adsorption models were tested to fit the experimental data (Table 3). The selection of the isotherm model was based on the highest determination coefficient (R^2) value (Table 3). The adsorption mechanisms differ depending on the triarylmethane molecule and the type of non-covalent interactions present in the aqueous medium (Figure 11). The adsorption of PR and FB onto the composite material fitted the BET model, which is based on multilayer adsorption. The C_{BET} parameter values are related to the adsorbent-adsorbate interactions and for the first adsorption layer [54], were 26.3 and 52 mg/L for PR and BF, respectively.

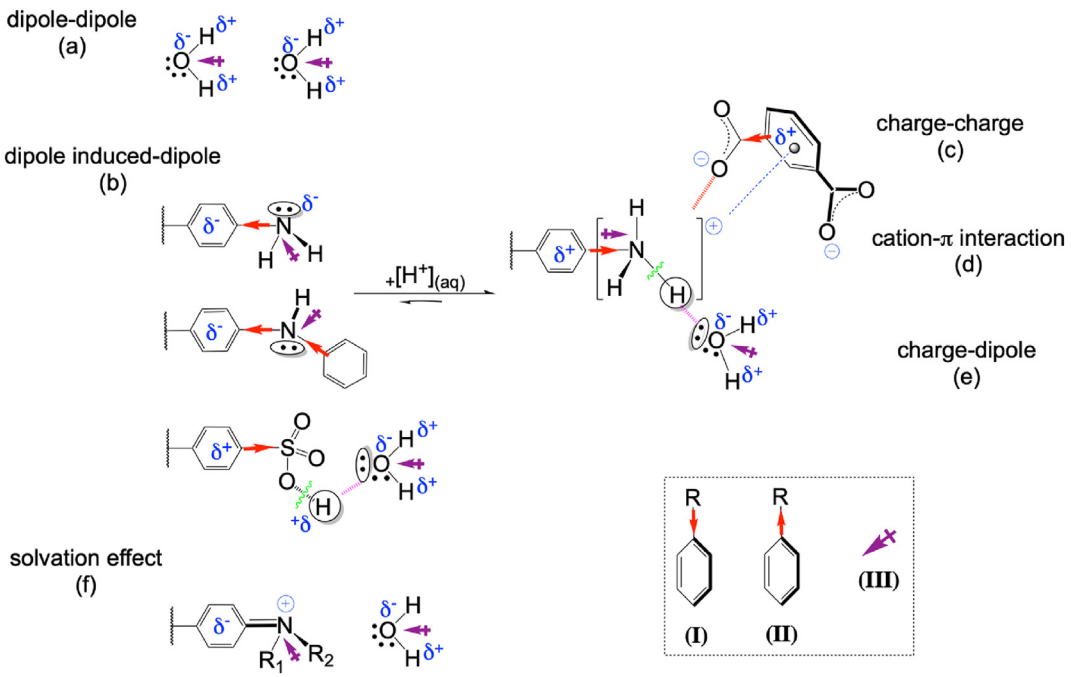

Figure 11. Possible non-covalent interactions by triarylmethane dyes in aqueous solution. Meaning of colored arrows: electron donating group: stabilizes the intermediate, activates the ring (I); electron withdrawing the intermediate, deactivates the ring (II); inductive effect ($_{+}$I) (III)).

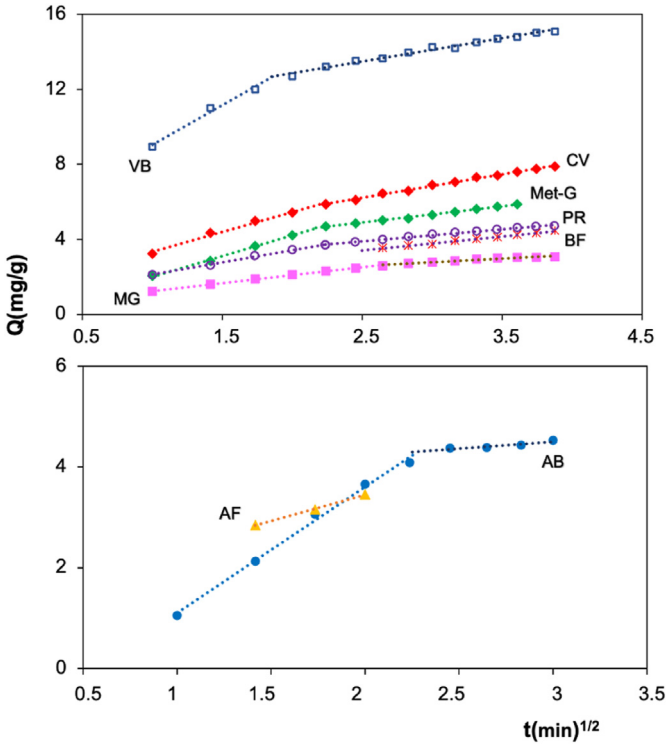

Figure 12. Intraparticle diffusion model study for the selected triarylmethane dye.

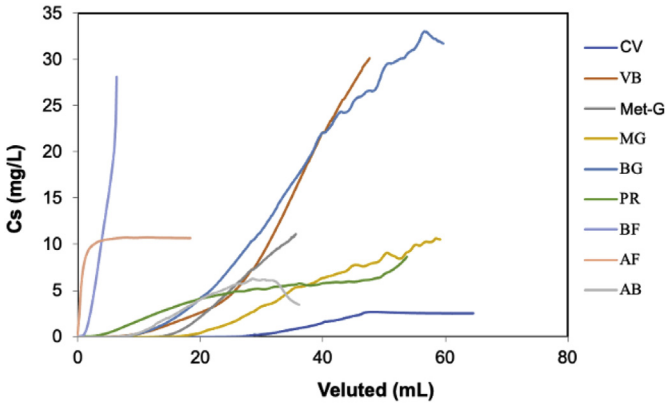

Figure 13. Breakthrough curve for triarylmethane dyes-Cotton@Fe-BTC.

The adsorption capacity (q_m) of the Cotton@Fe-BTC was found to be q_m (mg/g): PR (2.40) < BF (6.85), which was probably an electron-donating *p*-methyl group. It can be seen that the MET isotherm model is the most appropriate one for the adsorption of MG, CV and Met-G with high (R^2) (>0.9600). The MET model includes the surface tension effects in the BET isotherm model. The q_m (mg/g) was found to be MG (1.53) < Met-G (2.05) ~ CV (2.07). Among the all-adsorption isotherms considered, the adsorption of BG and AF was shown to fit the Khan isotherm model. Khan's empirical model considers the combination of two adsorption models: the Langmuir and Freundlich models. Even though the adsorption may be driven by steric hindrance of AF dye molecules, other interactions should not be ignored as it was pointed out in Figures 9 and 11 and explained above [55]. The BG adsorption process exhibits the fastest removal/adsorption onto Cotton@Fe-BTC at working conditions and Cotton@Fe-BTC favorably adsorbed BG. The Freundlich isotherm (R^2 = 0.9647) provided the best fit for its adsorption mechanisms. The model assumes multilayer adsorption on a heterogeneous adsorbent surface, involving non-ideal and reversible adsorption on active sites with an exponential energy distribution [56].

The value of 1/n indicates the favorability of adsorption, when $n < 1$ the adsorption conditions are favorable and chemisorption is involved.

Moreover, it is seen that the Koble-Corrigan model was the most suitable for AB dye adsorption. The results show that a combination of different uptake mechanisms occurred in AB dye adsorption by the synthesized Cotton@Fe-BTC fibers. The Koble-Corrigan model's parameter B value is negative, indicating that the adsorption of AB dye by

Table 3. Equation parameters of isotherm models for the selected triarylmethane dye onto Cotton@Fe-BTC.

Dye	Parameters	R^2	Model	Formula
MG	q_{sm} = 1.53 mg/g k = 29.2 mg/L C_e = 12.35 mg/L	0.9983	MET	$q_e = q_{sm}\left(\frac{k}{\ln\left(\frac{C_e}{C_s}\right)}\right)^{1/3}$
CV	q_{sm} = 2.07 mg/g k = 100.6 mg/L C_e = 10 mg/L	0.9688		
Met-G	q_{sm} = 2.05 mg/g k = 23.65 mg/L C_e = 10 mg/L	0.9769		
BG	k_f = 2.57 mmol/kg n_F = 4.37	0.9647	Freundlich	$q_e = k_f C_e^{1/n_F}$
VB	q_{sm} = 5.44 mg/g C_k = 37.47 mg/L a_k = 0.719 mg/L	0.9914	Khan	$q_e = \frac{q_{sm} C_k C_e}{(1 + b_k C_e)^{a_k}}$
AF	C_k = 0.5793 mg/L a_k = 0.2078 mg/L	0.9977		
AB	A = 0.9396 k_f = 2.57 mg/g n_F = 4.37 mg/L C_e = 0.0826 mg/L B = -0.6126 mg/L	0.9824	Koble-Corrigan	$q_e = \frac{A C_e^{n_k}}{1 + B C_e^{n_k}}$
PR	q_m = 6.85 mg/g C_{BET} = 26.3 mg/L C_e = 5.682 mg/L	0.9969	BET	$q_e = \frac{q_{mBET} C_{BET} C_e}{(C_e - C_s)\left[1 + (C_{BET^{-1}})\frac{C_e}{C_s}\right]}$
BF	q_m = 2.40 mg/mg C_{BET} = 52 mg/L C_e = 29.55 mg/L	0.9852		

C is the dye concentration (mg/L), Q_0 (mg/g) is the monolayer adsorption capacity of the adsorbent, *Q* (mg/·g) is the amount of dye adsorbed (mg/g), K_L (L/mg) Langmuir constant and K_F Freundlich equilibrium constant ((mg/g)·(L/mg)$^{1/n}$). *Cs* adsorbate monolayer saturation concentration (mg/L), q_m (mg/g) is the amount of dye adsorbed in forming a complete monolayer, C_{nBET}n-layer BET constant,·K_b indicates a BET constant explaining the energy of interaction with the surface. q_{SM} (mg/g) MET theoretical isotherm saturation capacity, q_{SK} (mg/g) Khan theoretical isotherm saturation capacity. A_{KC}, B_{KC}, and β are Koble-Corrigan isotherm constants.

Cotton@Fe-BTC fibers was not efficient. In agreement with the above findings, the structural tension observed in the AF dye led to a significant destabilization of this dye in the aqueous solution and its low retention by the Cotton@Fe-BTC network.

4. Conclusions

We have developed a procedure of synthesis of Cotton@Fe-BTC without the drawbacks of low adsorption capacity, poor selectivity, complex preparation processes, and difficulty to be regenerated that other adsorbent suffer from. Further major advantages of this synthetic process are that it is low cost and environmentally friendly. The adsorptive properties of Cotton@Fe-BTC have been evaluated by applying it to the adsorption of triarylmethane dye from aqueous solutions. The results reported here confirm that Cotton@Fe-BTC is a highly efficient adsorbent for this dye, which are difficult to be degraded in natural environments. The maximum adsorption capacities ranged from 1.53 mg/g (MG) to 6.85 mg/g (PR). Kinetic studies revealed that the adsorption process is very fast (<20 min) and that it takes place in two steps: first- and second-order rate kinetics are involved in the first and second stages, respectively. Column studies revealed the percentage of saturation to be equal or higher than 90%. Hydrated protons $[H(H_2O)_n]^+$ are proposed to be participant in the adsorption of anionic dye results. The results and discussion provide a new proof-of concept prospect for water is a suitable media for the triphenylmethane dye adsorption, as well as participant; being involved for adsorption of the anionic dye on the negative composite surface. These proposals support the suitability of the BET, MET, Freundlich, Khan and Koble-Corrigan multilayer adsorption models to explain the adsorption isotherms data for the corresponding dye. Thus, in terms of applicability, we proposed a new adsorbent material, Cotton@Fe-BTC composite, that can be highly effective in removing dye from an aqueous solution. The results presented here have significant environmental applications in that they can be applied to the control of triarylmethane dye from textile or other industrial effluents that are released into the environment.

Declarations

Author contribution statement

Conde-González J.E.: Conceived and designed the experiments; Performed the experiments.

Lorenzo-Luis, P.: Analyzed and interpreted the data; Wrote the paper.

Salvadó V; Havel J.: Analyzed and interpreted the data.

Peña-Méndez E.M.: Conceived and designed the experiments; Performed the experiments; Wrote the paper.

Funding statement

This work was supported by the Ministry of Economy and Competitivity (Spain), project Ref. MAT2017-89207-R.

Data availability statement

Data included in article/supplementary material/referenced in article.

Declaration of interests statement

The authors declare no conflict of interest.

Additional information

Supplementary content related to this article has been published online at https://doi.org/10.1016/j.heliyon.2021.e08524.

References

[1] M. Berradi, R. Hsissou, M. Khudhair, M. Assouag, O. Cherkaoui, A. El Bachiri, A. El Harfi, Textile finishing dye and their impact on aquatic environs, Heliyon 5 (2019), e02711.

[2] B. Lellis, C.Z. Fávaro-Polonio, J.A. Pamphile, J.C. Polonio, Effects of textile dye on health and the environment and bioremediation potential of living organisms, Biotechn. Res. Innov. 3 (2019) 275–290.

[3] A.S. Sartape, A.M. Mandhare, V.V. Jadhav, P.D. Raut, M.A. Anuse, S.S. Kolekar, Removal of malachite green dye from aqueous solution with adsorption technique using Limonia acidissima (wood apple) shell as low cost adsorbent, Arab. J. Chem. 10 (2017) S3229–S3238.

[4] B.K. Nandi, A. Goswani, M.K. Purkait, Adsorption characteristics of brilliant green dye on kaolin, J. Hazard Mater. 161 (2009) 387–395.

[5] A. Mittal, R. Ahmad, I. Hasan, Iron oxide-impregnated dextrin nanocomposite: synthesis and its application for the biosorption of Cr(VI) ions from aqueous solution, Desalin. Water Treat. 57 (2016) 15133–15145.

[6] A. Murray, B. Örmeci, Competitive effects of humic acid and wastewater on adsorption of Methylene Blue dye by activated carbon and non-imprinted polymers, J. Environ. Sci. 66 (2018) 310–317.

[7] M. Shaban, M.R. Abukhadra, M.G. Shahien, S.S. Ibrahim, Novel bentonite/zeolite-NaP composite efficiently removes methylene blue and Congo red dye, Environ. Chem. Lett. 16 (2018) 275–280.

[8] S.S. Thair, N. Rauf, Removal of a cationic dye from aqueous solutions by adsorption onto bentonite clay, Chemosphere 63 (2006) 1842–1848.

[9] N.T.T. Tu, T.V. Thien, P.D. Du, V.T.T. Chau, T.X. Mau, D.Q. Khieu, Adsorptive removal of Congo red from aqueous solution using zeolitic imidazolate framework–67, J. Environ. Chem. Engineering 6 (2018) 2269–2280.

[10] N. López-Gutiérrez, R. Romero-González, J.L.M. Vidal, A.G. Frenich, Analysis of triphenylmethane dye in seafood products: a review of extraction methods and determination by liquid chromatography coupled to mass spectrometry, Anal. Methods 5 (2013) 3434–3449.

[11] S. Horike, S. Kitagawa, Metal-organic frameworks: applications from catalysis to gas storage, in: David Farrusseng (Ed.), Wiley-VCH Verlag GmbH & Co. KGaA. Wiley-VCH Verlag GmbH & Co. KGaA, first ed., 2011, pp. 3–22.

[12] L. Ma, W. Lin, Designing metal-organic frameworks for catalytic applications, Top. Curr. Chem. 293 (2010) 175–205.

[13] C.B. Aakeroy, N.R. Champness, C. Janiak, Recent advances in crystal engineering, CrystEngComm 12 (2010) 22–43.

[14] O.M. Yaghi, H. Li, T.L. Groy, Construction of porous solids from hydrogen-bonded metal complexes of 1,3,5-benzenetricarboxylic acid, J. Am. Chem. Soc. 118 (1996) 9096–9101.

[15] C. Janiak, J.K. Vieth, MOFs, MILs and more: concepts, properties and applications for porous coordination networks (PCNs), New J. Chem. 34 (2010) 2366–2388.

[16] M. Bellusci, P. Guglielmi, A. Masi, F. Padella, G. Singh, N. Yaacoub, D. Peddis, D. Secci, Magnetic Metal−Organic framework composite by fast and facile mechanochemical process, Inorg. Chem. 57 (2018) 1806–1814.

[17] R.A.S. Rmit, Chemistry and structure of cellulosic fibers as reinforcements in natural fiber composites, Natural Fiber Composites (2014) 66–83.

[18] M. Tavakolian, S.M. Jafari, T.G.M. van de Ven, A review on surface-functionalized cellulosic nanostructures as biocompatible antibacterial materials, Nano-Micro Lett. 12 (2020) 73–95.

[19] M. da Silva Pinto, C. Augusto Sierra-Avila, J.P. Hinestroza, In situ synthesis of a Cu-BTC metal–organic framework (MOF 199) onto cellulosic fibrous substrates: cotton, Cellulose 19 (2012) 1771–1779.

[20] R.M. Abdelhameed, H. Abdel-Gawad, M. Elshahat, H.E. Emam, Cu–BTC@cotton composite: design and removal of ethion insecticide from water, RSC Adv. 6 (2016) 42324–42333.

[21] Y. Sua, S. Wanga, N. Zhanga, P. Cuia, Y. Gaoa, T. Baoa, Zr-MOF modified cotton fiber for pipette tip solid-phase extraction of four phenoxy herbicides in complex samples, Ecotoxicol. Environ. Saf. 201 (2020) 110764–110771.

[22] T. Bao, Y. Su, N.Z.Y. Gao, S. Wang, Hydrophilic carboxyl cotton for in situ growth of UiO-66 and its application as adsorbents, Ind. Eng. Chem. Res. 58 (2019) 20331–20339.

[23] A. Yang, Z. Wang, Y. Zhu, Facile preparation and adsorption performance of low-cost MOF@ cotton fiber composite for uranium removal, Sci. Rep. 10 (2020) 19271–19281.

[24] H.E. Emam, H.B. Ahmed, E. Gomaa, M.H. Helal, R.M. Abdelhameed, Recyclable photocatalyst composites based on Ag_3VO_4 and Ag_2WO_4@MOF@cotton for effective discoloration of dye in visible light, Cellulose 27 (2020) 7139–7155.

[25] V.K.-M. Au, Recent advances in the use of metal-organic frameworks for dye adsorption, Front. Chem. 8 (2020) 708–715.

[26] B. Parmar, K.K. Bisht, G. Rajput, E. Suresh, Recent advances in metal–organic frameworks as adsorbent materials for hazardous dye molecules, Dalton Trans. 50 (2021) 3083–3108.

[27] I.E. Uflyand, V.A. Zhinzhilo, V.O. Nikolaevskaya, B.I. Kharisov, C.M.O. González, O.V. Kharissova, Recent strategies to improve MOF performance in solid phase extraction of organic dye, Microchem. J. 168 (2021) 106387–106411.

[28] E.M. Peña-Méndez, R.M. Mawale, J.E. Conde-González, B. Socas-Rodríguez, J. Havel, C. Ruiz-Pérez, Metal organic framework composite, nano-Fe_3O_4@Fe-(benzene-1,3,5- tricarboxylic acid), for solid phase extraction of blood lipid regulators from water, Talanta 207 (2020) 120275–120282.

[29] Z. Ling, S. Chen, X. Zhang, K. Takabe, F. Xu, Unraveling variations of crystalline cellulose induced by ionic liquid and their effects on enzymatic hydrolysis, Sci. Rep. 7 (2017) 10230–12240.

[30] M. Sánchez-Sanchez, I. de Asua, D. Ruano, K. Díaz, Direct synthesis, structural features and enhanced catalytic activity of the Basolite F300-like semi-amorphous Fe-BTC framework, Cryst. Growth Des. 15 (2015) 4498–4506.

[31] A.F. Sapnik, I. Bechis, S.M. Collins, D.N. Johnstone, G. Divitini, A.J. Smith, P.A. Chater, M.A. Addicoat, T. Johnson, D.A. Keen, K.E. Jelfs, T.D. Bennett, Mixed hierarchical local structure in a disordered metal–organic framework, Nat. Commun. 12 (2021) 2062–2073.

[32] G. Mahalakshmi, V. Balachandran, FT-IR and FT-Raman spectra, normal coordinate analysis and ab initio computations of Trimesic acid, Spectrochim. Acta Mol. Biomol. Spectrosc. 124 (2014) 535–547.

[33] D.J. Xiao, E.D. Bloch, J.A. Mason, W.L. Queen, M.R. Hudson, N. Planas, J. Borycz, A.L. Dzubak, P. Verma, K. Lee, F. Bonino, V. Crocella, J. Yano, S. Bordiga, D.G. Truhlar, L. Gagliardi, C.M. Brown, J.R. Long, Oxidation of ethane to ethanol by N_2O in a metal–organic framework with coordinatively unsaturated iron(II) sites, Nat. Chem. 6 (2014) 590–595.

[34] R. Anand, F. Borghi, F. Manoli, I. Manet, V. Agostoni, P. Reschiglian, R. Gref, S. Monti, Host−Guest interactions in Fe(III)-Trimesate MOF nanoparticles loaded with doxorubicin, J. Phys. Chem. B 118 (2014) 8532–8539.

[35] P. Horcajada, S. Surblé, C. Serre, D.-Y. Hong, Y.-K. Seo, J.-S. Chang, J.-M. Grenéche, I. Margiolakid, G. Féreya, Synthesis and catalytic properties of MIL-100(Fe), an iron(III) carboxylate with large pores, Chem. Commun. (2007) 2820–2822.

[36] A. Dhakshinamoorthy, M. Alvaro, P. Horcajada, E. Gibson, M. Vishnuvarthan, A. Vimont, J.-M. Grenéche, C. Serre, M. Daturi, H. Garcia, Comparison of porous iron trimesates basolite F300 and MIL-100(Fe) as heterogeneous catalysts for lewis acid and oxidation reactions: roles of structural defects and stability, ACS Catal. 2 (2012) 2060–2065.

[37] S. Ciattini, F. Costantino, P. Lorenzo-Luis, S. Midollini, A. Orlandini, A. Vacca, Inorganic-organic hybrids formed by P,P′-Diphenylmethylenediphosphinate, pcp^{2-}, with the Cu^{2+} ion. X-Ray crystal structures of $[Cu(pcp)(H_2O)2]\cdot H_2O$ and $[Cu(pcp)(bipy)(H_2O)]$, Inorg. Chem. 44 (2005) 4008–4016.

[38] M.C. Das, S.B. Maity, P.K. Bharadwaj, Supramolecular association of water molecules forming discrete clusters in the voids of coordination polymers, Curr. Opin. Solid State Mater. Sci. 13 (2009) 76–90.

[39] K.O. Otun, Temperature-controlled activation and characterization of iron-based metalorganic frameworks, Inorg. Chim. Acta. 507 (2020) 119563–119567.

[40] P. Qin, Y. Yang, X. Zhang, J. Niu, H. Yang, S. Tian, J. Zhu, M. Lu, Highly efficient, rapid, and simultaneous removal of cationic dye from aqueous solution using monodispersed mesoporous silica nanoparticles as the adsorbent, Nanomaterials 8 (2018) 1–14.

[41] R. Nvetha, R.P. Kollu, K. Chandar, S. Pitchaimuthu, S.K. Jeong, A.N. Grace, Role of MIL-53(Fe)/hydrated–dehydrated MOF catalyst for electrochemical hydrogen evolution reaction (HER) in alkaline medium and photocatalysis, RSC Adv. 9 (2019) 3215–3223.

[42] J.E. Conde-González, E.M. Peña-Méndez, A.M. Melián-Fernández, J. Havel, V. Salvadó, Synthesis, performance and mechanism of nanoporous Fe-(1,3,5-tricarboxylic acid) metal-organic framework in the removal of anionic dye from water, Environ. Nanotechn. Monitor. Manag. 16 (2021) 100541–100549.

[43] J. Havel, E. Högfeldt, Computer evaluation of water sorption ion exchangers, Talanta 39 (1992) 517–522.

[44] L.K. Tsou, C.D. Tatko, M.L. Waters, Simple cation- π interaction between a phenyl ring and a protonated amine stabilizes an α-helix in water, J. Am. Chem. Soc. 124 (2002) 14917–14921.

[45] P.A. Sims, C.F. Wong, D. Vuga, J.A. McCammon, B.M. Sefton, Relative contributions of desolvation, inter- and intramolecular interactions to binding affinity in protein kinase systems, J. Comput. Chem. 26 (2005) 668–681.

[46] Y.-L. Ma, M. Quan, X.-L. Lin, Q. Cheng, H. Yao, X.-R. Yang, M.-S. Li, W.- Er Liu, L.-M. Bai, R. Wang, W. Jiang, Biomimetic recognition of organic drug molecules in water by amide naphthotubes, CCS Chem 2 (2020) 1078–1092.

[47] Y.S. Al-Degs, M.A.M. Khraisheh, S.J. Allen, M.N. Ahmad, Adsorption characteristics of reactive dyes in columns of activated carbon, J. Hazard Mater. 165 (2009) 944–949.

[48] F. Leng, W. Wang, X.J. Zhao, X.L. Hu, Y.F. Li, Adsorption interaction between a metal–organic framework of chromium–benzenedicarboxylates and uranine in aqueous solution, Colloid. Surface. Physicochem. Eng. Aspect. 441 (2014) 164–169.

[49] M. Ganguly, P.A. Ariya, Novel technology for the removal of brilliant green from water: influence of post-oxidation, environmental conditions, and capping, ACS Omega 4 (2019) 12107–12120.

[50] J.E. Conde-González, E.M. Peña-Méndez, S. Rybáková, J. Pasán, C. Ruiz-Pérez, J. Havel, Adsorption of silver nanoparticles from aqueous solution on copper-based metal organic frameworks (HKUST-1), Chemosphere 150 (150) (2016) 659–666.

[51] R. Kumar, M.O. Ansari, M.A. Barakat, Adsorption of brilliant green by surfactant doped polyaniline/MWCNTs composite: evaluation of the kinetic, thermodynamic, and isotherm, Ind. Eng. Chem. Res. 53 (2014) 7167–7175.
[52] R. Saadi, Z. Saadi, R. Fazaeli, N.E. Fard, Monolayer and multilayer adsorption isotherm models for sorption from aqueous media, Kor. J. Chem. Eng. 32 (2015) 787–799.
[53] K.Y. Foo, B.H. Hameed, Insights into the modeling of adsorption isotherm systems, Chem. Eng. J. 156 (2010) 2–10.
[54] B. Singha, S.K. Das, Adsorptive removal of Cu(II) from aqueous solution and industrial effluent using natural/agricultural wastes, Colloids Surf. B Biointerfaces 107 (2013) 97–106.
[55] A.A. Adeyemo, I.O. Adeoye, O.S. Bello, Metal organic frameworks as adsorbents for dye adsorption: overview, prospects and future challenges, Toxicol. Environ. Chem. 94 (2012) 1846–1863.
[56] P. Monash, G. Pugazhenthi, Adsorption of crystal violet dye from aqueous solution using mesoporous materials synthesized at room temperature, Adsorption 15 (2009) 390–405.